LiDAR-camera Calibration in an Uniaxial 1-DoF Sensor System

Tamás Tófalvi, Bandó Kovács, Levente Hajder and Tekla Tóth
Department of Algorithms and their Applications, Eötvös Loránd University, Pázmány Péter stny. 1/C, Budapest 1117, Hungary

Keywords: LiDAR-camera Calibration, Extrinsic Parameter Estimation, Linear Problem.

Abstract: This paper introduces a novel camera-LiDAR calibration method using a simple planar chessboard pattern as the calibration object. We propose a special mounting for the sensors when only one rotation angle should be estimated for the calibration. It is proved that the calibration can optimally be solved in the least-squares sense even if the problem is overdetermined, *i.e.*, when many chessboard patterns are visible for the sensors. The accuracy and precision of our unique solution are validated on both simulated and real-world data.

1 INTRODUCTION

Nowadays, LiDAR sensors have frequently appeared in visual systems. They are very popular in autonomous vehicles despite their high price. The output of digital cameras and radar sensors can also expand the visual information for autonomous driving.

In the opinion of many researchers, including us, digital cameras and LiDARs complement each other. Basic geometric objects such as planes, spheres, cylinders can be very efficiently estimated on point clouds, scanned by LiDARs, while more complex objects can be detected in digital images.

Several methods have been proposed to calibrate a camera-LiDAR sensor pair. *E.g.* the pioneering work of (Zhang and Pless, 2004) deals with 2D laser and camera calibration. The state-of-the-art methods for 3D LiDAR calibration can be divided into the following groups overviewed in Figure 1:

Planar-object-based: Many algorithms apply different form of planar surfaces. The main difficulty is the accurate detection of the plane borders. Therefore, the precision for estimating the translation between the devices can be very low. A trivial solution is to apply multiple non-parallel planes (Park et al., 2014; Veĺas et al., 2014; Gong et al., 2013; Pusztai et al., 2018) to accurately estimate the translation between the sensors.

Chessboard-based: Some methods (Geiger et al., 2012; Pandey et al., 2010; Zhou et al., 2018) use planar chessboards as they are very efficient for camera calibration (Zhang, 2000), but other patterns (Rodriguez F et al., ; Alismail et al., 2012) can be applied as well. The drawback of these pattern-based approaches is the detection in 3D point cloud: only the plane orientations can be precisely identified, the plane locations cannot.

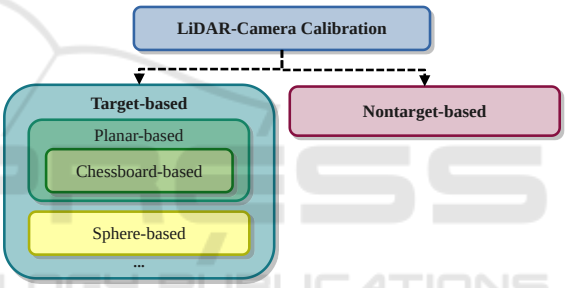

Figure 1: The overview of the related calibration methods.

Sphere-based: Spherical objects (Tóth et al., 2020) are also useful for camera-LiDAR calibration. The difficulty is that they require a regular and large spherical surface, which is not easy to manufacture.

Nontarget-based: Many methods (Frohlich et al., 2016; Pandey et al., 2012) are using no calibration objects at all. These methods provide a general solution, as they don't require specialised objects to present in the environment, however the accuracy of these is not as good as the target-based methods'.

The main practical problem of calibration is that if the cameras and LiDAR devices are mounted on *e.g.* a vehicle, the orientation/viewpoint can be changed during operation due to vibration. Therefore, recalibration is required.

In this paper, we simplify the calibration problem to solving a 1-DoF system as displayed in Figure 2 schematically. During the real-world tests, the camera

Tófalvi, T., Kovács, B., Hajder, L. and Tóth, T.
LiDAR-camera Calibration in an Uniaxial 1-DoF Sensor System.
DOI: 10.5220/0010988800003124
In *Proceedings of the 17th International Joint Conference on Computer Vision, Imaging and Computer Graphics Theory and Applications (VISIGRAPP 2022) - Volume 4: VISAPP*, pages 730-738
ISBN: 978-989-758-555-5; ISSN: 2184-4321

and the LiDAR can be fixed by a special 3D printed fixture as in Figure 5. This mounting guarantees that the vertical axes of the camera and LiDAR are parallel and the relative locations are fixed. As a consequence, the Degrees of Freedom (DoF) for the problem is one: it is given by the angle of rotation around this vertical axis.

The proposed algorithm is a *Chessboard-based* calibration process that requires only one checkerboard pattern. Nonetheless, the accuracy is higher if more boards are available. Therefore, the method can be used to re-calibrate the equipment if there is at least one checkerboard around it. A snapshot of the tested calibration environment is in Figure 5.

Contribution. A novel Camera-LiDAR calibration method is proposed here. We apply a special fixation that reduces the DoFs of the problem from six to one. The proposed estimator can handle the minimal and over-determined cases as well. Chessboards are used for the calibration as their plane can be efficiently detected on both LiDAR point clouds and camera images. Real-world tests show that the estimation is accurate enough.

The source code and the printable 3D model of the camera-LiDAR fixation will be available on our webpage in case of paper acceptance.

2 PROPOSED METHOD

In this section, we propose a novel method for calibrating a LiDAR-camera system with only one DoF. The general extrinsic calibration problem is to estimate the rigid body transformation between the LiDAR and camera. This transformation is composed of an $\mathbf{R} \in \mathbb{R}^{3\times3}$ rotation matrix and a $\mathbf{t} = \begin{bmatrix} t_X & t_Y & t_Z \end{bmatrix}^T$ translation vector. The rotation matrix can be written as the product of three rotations around the X, Y and Z axes: $\mathbf{R} = \mathbf{R}_X \cdot \mathbf{R}_Y \cdot \mathbf{R}_Z$.

During the extrinsic calibration, a pinhole camera model is assumed with perspective mapping. To map a 3D point given in the LiDAR coordinate system $\mathbf{p}_L = \begin{bmatrix} p_x & p_y & p_z \end{bmatrix}^T$ onto the image, $\mathbf{p}_L$ is transformed by the rotation $\mathbf{R}$ and the translation $\mathbf{t}$. Thereafter, the position of the point is in the camera coordinate system $\mathbf{p}_C = \mathbf{R}(\mathbf{p}_L - \mathbf{t})$. From the camera coordinate system we can project the point onto the image plane by applying a $\mathbf{K} \in \mathbb{R}^{3\times3}$ transformation containing the intrinsic camera parameters. Given f focal distance, k_u, k_v pixel sizes and $\begin{bmatrix} u_0 & v_0 \end{bmatrix}^T$ principal point the projection matrix $\mathbf{K}$ will have the form

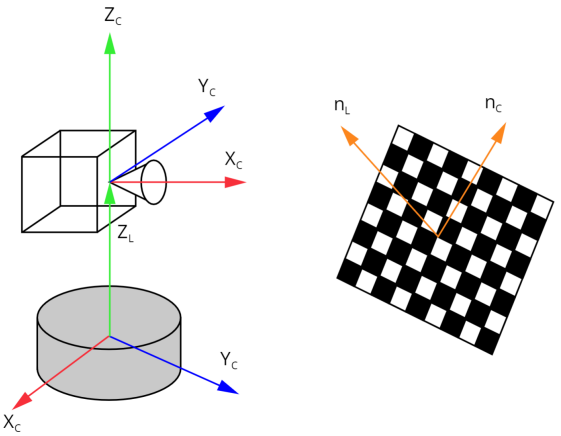

Figure 2: Schematic figure of Camera-LiDAR setup. Coordinate sytems are highlighted by red, green and blue colors. The main goal is to estimate the rotation around axis Z_C.

$$\mathbf{K} = \begin{bmatrix} fk_u & 0 & u_0 \\ 0 & fk_v & v_0 \\ 0 & 0 & 1 \end{bmatrix}. \tag{1}$$

Finally, selecting the world coordinate system as the own coordinate system of the LiDAR, we get the relationship between the points of LiDAR point cloud and pixels of the image. The pixel coordinates of the original 3D point are

$$\begin{bmatrix} u \\ v \\ 1 \end{bmatrix} \sim \mathbf{K} \cdot \mathbf{R}(\mathbf{p}_L - \mathbf{t}). \tag{2}$$

2.1 Restrictions

The method considers the pinhole camera model and known intrinsic camera parameters.

The novelty of the proposed method comes from our own 3D printed mount which connects the camera on the top of the LiDAR. This connection allows us to make several restrictions about the systems which in turn will reduce the complexity of the extrinsic calibration problem to approximating a single rotation (1-DoF problem). The mounted LiDAR-camera system can be seen in Figure 5.

The first restriction is the coincidence of the vertical axes of the LiDAR and camera coordinate systems. This means, that given the basis vectors of the LiDAR coordinate systems X_L, Y_L, and Z_L; the basis vectors of the camera coordinate system X_C, Y_C, and Z_C, assuming that Z_L and Z_C are the coinciding vertical axes[1]: the planes spanned by X_L, Y_L and X_C,

[1] An important observation is that usually in the camera coordinate system the Z axis points forward, the Y axis is the vertical pointing down and the X axis points to the right. In our case, the camera coordinate system is as in Figure 2.

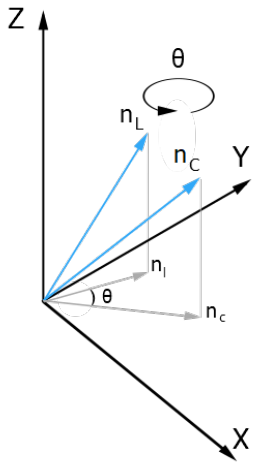

Figure 3: The goal of our calibration method is to estimate the rotation angle θ around axis Z.

Y_C respectively are parallel to each other illustrated in Figure 2. This yields to the equality of the rotations around the X and Y to the identity transformation $\mathbf{R}_X = \mathbf{R}_Y = \mathbf{I}$. The free parameter of the rotation came only from the rotation around the vertical Z axis:

$$\mathbf{R} = \mathbf{R}_Z(\theta) = \begin{bmatrix} \cos\theta & -\sin\theta & 0 \\ \sin\theta & \cos\theta & 0 \\ 0 & 0 & 1 \end{bmatrix}. \quad (3)$$

Our second restriction is, that the translation vector $\mathbf{t} = \begin{bmatrix} 0 & 0 & t_Z \end{bmatrix}^T$ is known from the schematics of the devices and the 3D printed mount.

The problem can be reduced to calculate a single rotation around the vertical axis, *i.e.*, angle θ if the camera matrix $\mathbf{K}$ and the one translation parameter t_z are known. Given these restrictions, Equation (2) modifies as follows

$$\begin{bmatrix} u \\ v \\ 1 \end{bmatrix} \sim \mathbf{K} \cdot \mathbf{R}_Z(\theta) \cdot \begin{bmatrix} p_x \\ p_y \\ p_z - t_z \end{bmatrix}. \quad (4)$$

2.2 Uniaxial Calibration

The target of the proposed extrinsic calibration method is a plane with a checkerboard pattern printed on it. This plane can be detected relatively easily on both the image and in the LiDAR point cloud.

After the plane detection, we calculate the normal vector of the checkerboard in both the LiDAR and camera coordinate system, these normal vectors are denoted as $\mathbf{n}_L$ and $\mathbf{n}_C$ respectively. The following equation holds between the two normal vectors: $\mathbf{n}_L = \mathbf{R}_Z \cdot \mathbf{n}_C$, which uses the same rotation as in Equation (3) visualized in Figure 3.

2.2.1 Plane Normal from the Point Cloud

At first, the plane points are selected manually. The output is a subset of the point cloud containing as few outliers as possible. This step is executed non-automatically, because the plane of the checkerboard is not necessarily the most prominent plane in the whole scene of the point cloud. After the point classification, the LO-RANSAC (Lebeda et al., 2012) algorithm can estimate the plane and its normal vector in the LiDAR coordinate system based on the candidate plane points.

2.2.2 Plane Normal from Image

In order to get the normal vector of checkerboard plane in the camera coordinate system, not all of the plane parameters are needed: a homography decomposition can determine the required normal vector.

The input of the homography estimation are two corresponding coplanar point sets. The first set of points are the detected checkerboard corners in the image of the camera. The second set of points will be in the form of $(0,0),(0,1),...,(1,0),(1,1),...,(n-1,m-1)$ (given a checkerboard pattern with size $n \times m$ and with unit length squares), derived from a virtual camera with an intrinsic matrix of $\mathbf{K} = \mathbf{I}$.

The homography matrix is defined by the $n \times m$ coplanar point pairs. The homography is estimated by the standard Direct Linear Transformation (DLT) technique (Hartley and Zisserman, 2003). This homography is decomposed as written in (Malis and Vargas, 2007), and the normal vector of the checkerboard in the camera coordinate system is obtained.

2.2.3 Rotation Form Normal Vectors

We determined the normal vector of the checkerboard in both the LiDAR and the camera coordinate systems: $\mathbf{n}_L = \begin{bmatrix} x & y & z \end{bmatrix}^T$ and $\mathbf{n}_C = \begin{bmatrix} x' & y' & z' \end{bmatrix}^T$. Because of our assumption that the horizontal planes of LiDAR and camera coordinate systems are parallel, the depth coordinate becomes $z = z'$. If the projection of the normal vectors to the horizontal plane are $\mathbf{n}_l = \begin{bmatrix} x & y \end{bmatrix}^T$ and $\mathbf{n}_c = \begin{bmatrix} x' & y' \end{bmatrix}^T$ (see in Figure 3), the equation of the rotation between the two vectors yields to

$$\mathbf{R}(\theta) \cdot \mathbf{n}_l = \begin{bmatrix} \cos\theta & -\sin\theta \\ \sin\theta & \cos\theta \end{bmatrix} \cdot \begin{bmatrix} x \\ y \end{bmatrix} = \begin{bmatrix} x' \\ y' \end{bmatrix} = \mathbf{n}_c. \quad (5)$$

The proper alignment and rotation of the coordinate systems is an implementation problem that highly depends on the available sensors, but is easily solvable by 90° degree rotations.

After rearranging the equation:

$$\begin{bmatrix} x & -y \\ y & x \end{bmatrix} \cdot \begin{bmatrix} \cos\theta \\ \sin\theta \end{bmatrix} = \begin{bmatrix} x' \\ y' \end{bmatrix}. \quad (6)$$

Let use the substitutions as follows

$$\mathbf{F} = \begin{bmatrix} x & -y \\ y & x \end{bmatrix}, \qquad \mathbf{g} = \begin{bmatrix} \cos\theta \\ \sin\theta \end{bmatrix}, \qquad \mathbf{h} = \begin{bmatrix} x' \\ y' \end{bmatrix}. \quad (7)$$

The unknown calibration parameter can be defined as the solution of the minimization problem $\arg\min_{\mathbf{g}} \|\mathbf{Fg} - \mathbf{h}\|_2$ subject to $\|\mathbf{g}\|_2 = 1$. An algorithm for computing the optimal result for this type of problems is given in the appendix. The optimal angle is obtained via calculating the roots of a four-degree polynomial.

One pair of images is sufficient to perform the calibration. Notwithstanding, an overdetermind scenario with more corresponding point cloud-image pairs can increase the precise approximation of the rotation. Assuming k number of image pairs, k normal vector pairs can be gathered after the LO-RANSAC process and the homography decomposition:

$$\mathbf{n}_{l,1} = \begin{bmatrix} x_1 & y_1 \end{bmatrix}^T, \ldots, \mathbf{n}_{l,k} = \begin{bmatrix} x_k & y_k \end{bmatrix}^T,$$
$$\mathbf{n}_{c,1} = \begin{bmatrix} x'_1 & y'_1 \end{bmatrix}^T, \ldots, \mathbf{n}_{c,k} = \begin{bmatrix} x'_k & y'_k \end{bmatrix}^T.$$

If k image pairs are considered, Equation 6 can be written as follows:

$$\begin{bmatrix} x_1 & -y_1 \\ y_1 & x_1 \\ \vdots & \vdots \\ x_k & -y_k \\ y_k & x_k \end{bmatrix} \cdot \begin{bmatrix} \cos\theta \\ \sin\theta \end{bmatrix} = \begin{bmatrix} x'_1 \\ y'_1 \\ \vdots \\ x'_k \\ y'_k \end{bmatrix}. \quad (8)$$

Finally, the method discussed in the appendix ensures the optimal solution for the only unknown calibration parameter θ.

3 EXPERIMENTAL RESULTS

Qualitative and quantitative testing of the proposed method was carried out on both real and virtually generated images and point clouds compared to a concurrent calibration process in MATLAB. In this section, we analyze the results and evaluate the precision of the tested approaches.

3.1 Real Data

We gathered point cloud-image pairs using a Veldoyne VLP-16 LiDAR and a Hikvision MV-CA020-20GC sensor with high-quality Fujinon SV-0614H lenses. The non-perspective distortion of the lenses is negligible. The camera was mounted on top of the LiDAR with our special 3D printed mount. The data were collected in different settings and with different chessboards. Five data sets were gathered in different places: in an office, in a garage, and in a parking lot with three different chessboards. The sizes are from 4×5 to 9×10. Some input images can be seen in Figure 4.

Table 1: Standard deviation of the calculated rotations on the different data sets measured in degrees. *One by one*: only a single image used for calibration; *One by one**: one image used, but outliers are filtered out; *10 imgs.*: overdetermined estimation run for 10 randomly selected images. The best result is highlighted in every test case.

Data set	*One-by-one*	*One-by-one**	*10 imgs.*
#1	12.1753	2.3022	**0.9759**
#2	27.2212	2.3786	**1.0583**
#3	38.5715	**0.6895**	1.0392
#4	0.9453	-	**0.4899**
#5	28.9916	**1.2363**	4.0653

3.1.1 Precision of Estimated Rotation Angle

The first experiment examines the precision of angle estimation. On every data set, the calibration was performed one by one on each image – point cloud pair.

Our quantitative evaluations are based on the standard deviation of the estimated angles. The results are listed in Table 1, where we concentrated on determining the precision of the results. Best results are highlighted by bold numbers in every scenario. The data were filtered from the outliers (illustrated in the boxplots as separated dots). To evaluate the precision, first, the angles are obtained one by one from LiDAR-camera pairs. Thus, the proposed method is called for the minimal case. Then ten chessboard planes are randomly selected, and the over-determined algorithm is performed. The best results are around 1° on average.

The boxplots of the angles are pictured in Figures 6 and 7. Remark, that there are no outliers for data set 4. The calculated rotation angles have a big standard deviation because of outliers in the data set. The outliers are filtered by boxplot, and the deviations are recalculated. We also performed the calibration on ten image-point cloud pairs at a time. From the filtered data set, 10 randomly selected pairs were taken multiple times, and a rotation angle was determined with them.

Based on this test, it is obvious that outlier filtering is important to obtain more precise results. We can also note that in most cases using 10 images to perform the calibration produces more accurate results.

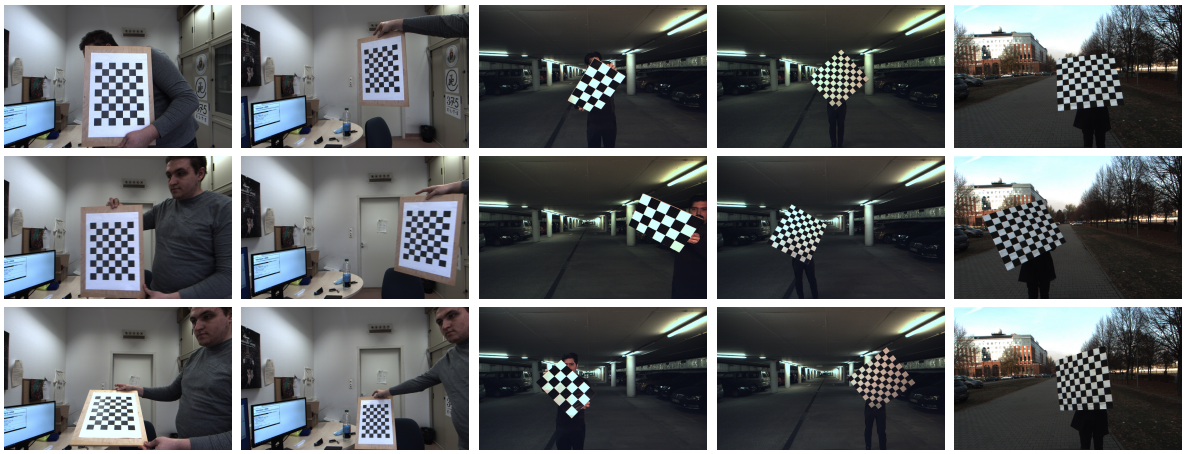

Data set 1 Data set 2 Data set 3 Data set 4 Data set 5

Figure 4: Some input image examples of the five different real data sets. The images and point clouds in data set 1 and 2 were taken in an office with a small 7x9 chessboard with 31mm square size. Data set 3 was gathered in a garage with a 60mm square sized 4x6 chessboard. With data set 4 and 5 we were using a large 81mm square sized 9x10 chessboard in a garage and in an outside parking lot.

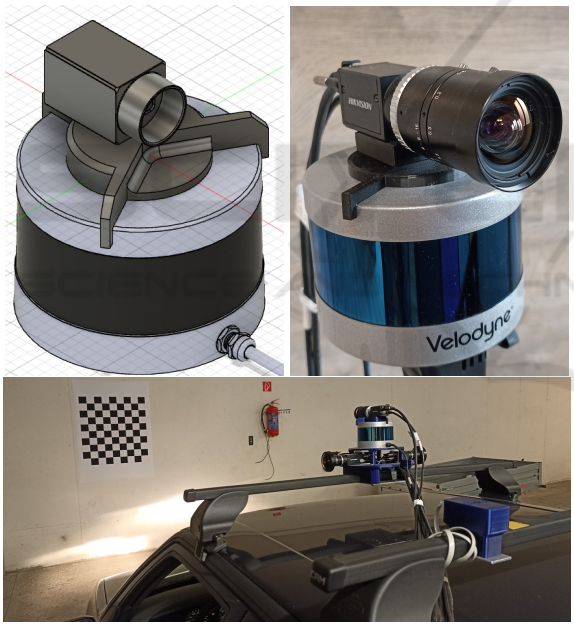

Figure 5: Camera-LiDAR setup. A special, 3D printed fixation used to connect the devices. **Top left:** 3D model of equipment. **Top rigth:** Realized Camera-LiDAR pair. **Bottom:** Proposed equipment mounted on the top of a car. A single chessboard is used for calibration.

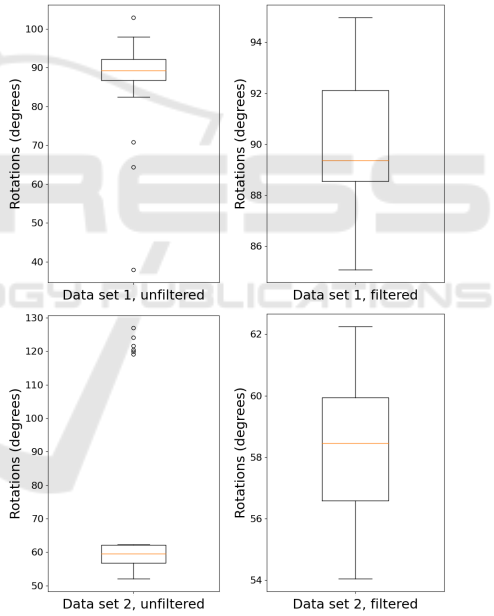

Figure 6: Boxplot of the rotations calibrated separately on each image pair before and after filtering, on data sets 1 and 2.

The resulting deviation values suggest that the need for re-calibration can be detected if the fixation error is larger than 1°–2°.

3.1.2 Point Cloud Colorization

We present the results of our extrinsic calibration method by point cloud colorization and projecting the points of the point cloud back to the image. LiDAR point clouds do not contain color information even if there is an intensity value for each point, however, they represent the reflectivity of the illuminated points. RGB color data can be retrieved from camera pixels if the LiDAR and camera are calibrated to each other. In these experiments, this calibration is carried out by the proposed method.

Figure 8 shows the examples when the LiDAR points are projected to the images. The chessboard-

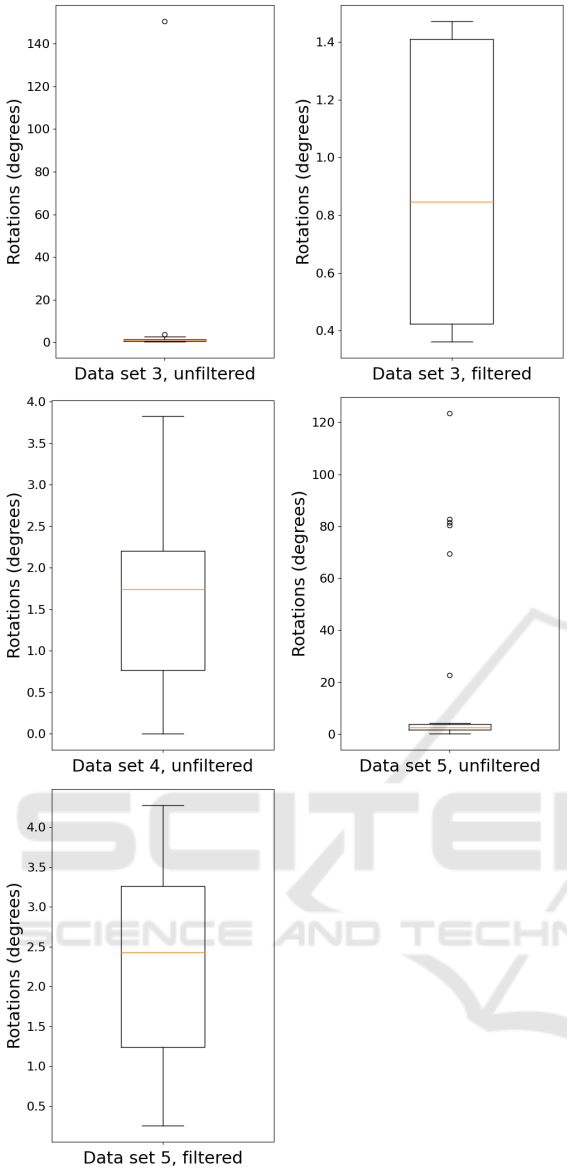

Figure 7: Boxplot of the rotations calibrated separately on each image pair before and after filtering, on data sets 3, 4 and 5. Note: on data set 4, no outliers were found.

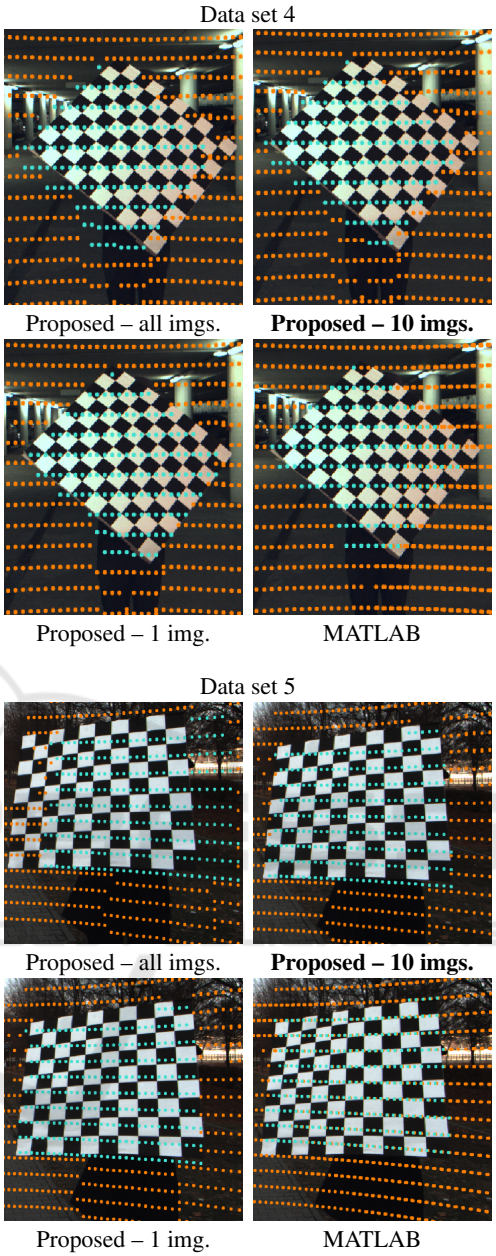

Figure 8: These images are from data set 4 and 5. After the calibration, the 3D points were projected back onto the image. The points corresponding to the chessboard plane can be seen in blue, all of the other back-projected LiDAR points are orange.

related points are colored by blue in the images. The accuracy of the results can be visually checked at the border of the chessboards. Colorized point clouds can also be seen in Figure 9.

We compared our results with the LiDAR-camera calibration toolbox (Zhou et al., 2018) of MATLAB. It is important to note, that this toolbox couldn't perform a calibration on several data sets, because of the low resolution of the LiDAR available. Our method does not have such problems.

Another important case is when the chessboard is on the wall as in Figure 5. This mounting does not affect our algorithm, because the only information we need is the normal vector of the plane of the chessboard in contrast to the MATLAB calibration method which is highly dependent on the size and orientation of the chessboard. The plane of the large wall can be detected by the well-known RANSAC (Fischler and Bolles, 1981) algorithm. In the future, the re-calibration and automatic detection of the chess-

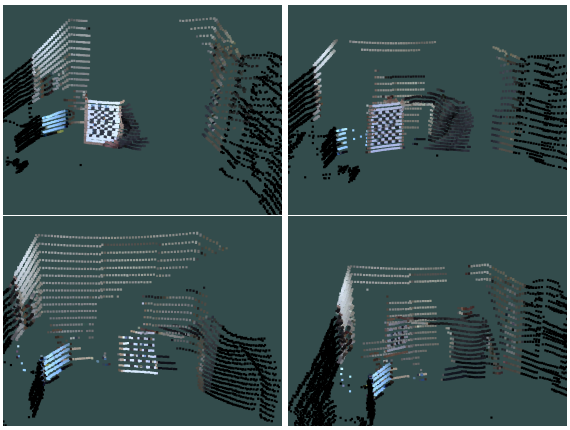

Figure 9: Colored point clouds on data sets 1 and 2 using the calibration results of the proposed method.

boards plane in the LiDAR point cloud can be solved this way, by assuming that the chessboard is mounted on the wall. The largest plane in front of the car will be that wall and detection of the chessboard can be enhanced by also using the intensity information of the scan.

3.2 Virtual Data

Multiple image and point cloud pairs were generated at different angles using Blensor [2]. The setup of the virtual camera and LiDAR can be seen in Figure 10. At each known rotation angle, we can evaluate the obtained rotation angle as the ground truth (GT) values are known from the simulator.

The results are seen in Table 2. Results for five different setups are compared, the ground truth angles are from 0° to 180°. The average error of the approximated rotation with the proposed extrinsic calibration method is only 0.1009°. It suggests that high-quality angle estimation is possible using the proposed calibration method.

Table 2: Calibration error of the proposed method on virtually generated data.

Rotation angle		Error
Ground truth	**Estimated**	
0°	0.0000°	0.0000°
45°	44.9032°	0.0976°
90°	89.6333°	0.3660°
135°	134.9589°	0.0410°
180°	179.9999°	$2.05° \times 10^{-7}$
Average error		0.1009°

[2]Blensor is an open source simulation package for LIDAR and Kinect sensors that cooperates with the computer vision tool Blender. See www.blensor.org for the details.

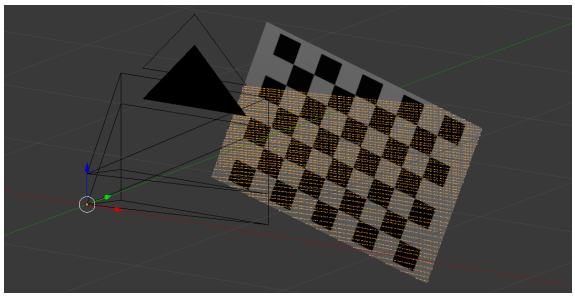

Figure 10: Setup of virtual LiDAR and camera in Blensor with chessboard and captured LiDAR point cloud.

4 CONCLUSION

In this paper, we proposed a novel camera-LiDAR calibration method, overviewed the restrictions of the test environment, and the main steps of our framework. In our setup, the camera is mounted on top of the LiDAR using a special 3D-printed fixation, and the DoF for calibration is reduced to one. We showed how this problem can be optimally solved in the least-squares sense. Both the minimal and the over-determined cases were discussed. For the minimal case, only one planar checkerboard pattern is required. We examined that the proposed method can be applied to recalibrate a camera-LiDAR setup if the fixation is changed during the vibration of the moving vehicles on which the devices are mounted. During synthetic and real-world tests, the proposed method had an error of around 1°.

ACKNOWLEDGEMENTS

Our work is supported by the project EFOP-3.6.3-VEKOP-16-2017- 00001: Talent Management in Autonomous Vehicle Control Technologies, by the Hungarian Government and co-financed by the European Social Fund. L. Hajder also thanks the support of the "Application Domain Specific Highly Reliable IT Solutions" project that has been implemented with the support provided from the National Research, Development and Innovation Fund of Hungary, financed under the Thematic Excellence Programme TKP2020-NKA-06 (National Challenges Subprogramme) funding scheme. T. Tófalvi has been supported by the ÚNKP-21-1 New National Excellence Program of the Ministry for Innovation and Technology from the source of the National Research, Development and Innovation fund.

REFERENCES

Alismail, H. S., Baker, L. D., and Browning, B. (2012). Automatic calibration of a range sensor and camera system. In *2012 Second Joint 3DIM/3DPVT Conference: 3D Imaging, Modeling, Processing, Visualization & Transmission (3DIMPVT 2012)*, Pittsburgh, PA. IEEE Computer Society.

Fischler, M. and Bolles, R. (1981). RANdom SAmpling Consensus: a paradigm for model fitting with application to image analysis and automated cartography. *Commun. Assoc. Comp. Mach.*, 24:358–367.

Frohlich, R., Kato, Z., Trémeau, A., Tamas, L., Shabo, S., and Waksman, Y. (2016). Region based fusion of 3d and 2d visual data for cultural heritage objects. In *23rd International Conference on Pattern Recognition, ICPR 2016, Cancún, Mexico, December 4-8, 2016*, pages 2404–2409.

Geiger, A., Moosmann, F., Car, O., and Schuster, B. (2012). Automatic camera and range sensor calibration using a single shot. In *IEEE International Conference on Robotics and Automation, ICRA 2012, 14-18 May, 2012, St. Paul, Minnesota, USA*, pages 3936–3943.

Gong, X., Lin, Y., and Liu, J. (2013). 3d lidar-camera extrinsic calibration using an arbitrary trihedron. *Sensors*, 13(2).

Hartley, R. I. and Zisserman, A. (2003). *Multiple View Geometry in Computer Vision*. Cambridge University Press.

Lebeda, K., Matas, J., and Chum, O. (2012). Fixing the locally optimized RANSAC. In *British Machine Vision Conference, BMVC 2012, Surrey, UK, September 3-7, 2012*, pages 1–11.

Malis, E. and Vargas, M. (2007). Deeper understanding of the homography decomposition for vision-based control. Research report.

Pandey, G., McBride, J., Savarese, S., and Eustice, R. (2010). Extrinsic calibration of a 3d laser scanner and an omnidirectional camera. In *7th IFAC Symposium on Intelligent Autonomous Vehicles*, volume 7, Leece, Italy.

Pandey, G., McBride, J. R., Savarese, S., and Eustice, R. M. (2012). Automatic targetless extrinsic calibration of a 3d lidar and camera by maximizing mutual information. In *Proceedings of the AAAI National Conference on Artificial Intelligence*, pages 2053–2059, Toronto, Canada.

Park, Y., Yun, S., Won, C. S., Cho, K., Um, K., and Sim, S. (2014). Calibration between color camera and 3d lidar instruments with a polygonal planar board. *Sensors*, 14(3):5333–5353.

Pusztai, Z., Eichhardt, I., and Hajder, L. (2018). Accurate calibration of multi-lidar-multi-camera systems. *Sensors*, 18(7):2139.

Rodriguez F, S., Fremont, V., and Bonnifait, P. Extrinsic calibration between a multi-layer lidar and a camera.

Tóth, T., Pusztai, Z., and Hajder, L. (2020). Automatic lidar-camera calibration of extrinsic parameters using a spherical target. In *2020 IEEE International Conference on Robotics and Automation (ICRA)*, pages 8580–8586.

Veĺas, M., Španěl, M., Materna, Z., and Herout, A. (2014). Calibration of rgb camera with velodyne lidar. In *WSCG 2014 Communication Papers Proceedings*, volume 2014, pages 135–144. Union Agency.

Zhang, Q. and Pless, R. (2004). Extrinsic calibration of a camera and laser range finder (improves camera calibration). In *2004 IEEE/RSJ International Conference on Intelligent Robots and Systems, Sendai, Japan, September 28 - October 2, 2004*, pages 2301–2306.

Zhang, Z. (2000). A flexible new technique for camera calibration. *IEEE Transactions on Pattern Analysis and Machine Intelligence*, 22(11):1330–1334.

Zhou, L., Li, Z., and Kaess, M. (2018). Automatic extrinsic calibration of a camera and a 3d lidar using line and plane correspondences. In *2018 IEEE/RSJ International Conference on Intelligent Robots and Systems, IROS 2018, Madrid, Spain, October 1-5, 2018*, pages 5562–5569.

APPENDIX

Solution of $\arg\min_{\mathbf{Y}} \|\mathbf{FG}-\mathbf{H}\|_2$ Subject to $\|\mathbf{g}\|_2 = 1$.

The objective is to show how the equation $\mathbf{Fg} = \mathbf{h}$ can be optimally solved, in the least squares sense, subject to $\mathbf{g}^{\mathrm{T}}\mathbf{g} = 1$. Cost function J can be written using Lagrangian multiplier λ as follows:

$$J = (\mathbf{Fg}-\mathbf{h})^{\mathrm{T}}(\mathbf{Fg}-\mathbf{h}) + \lambda \mathbf{g}^{\mathrm{T}}\mathbf{g}.$$

The optimal solution is given by the derivative of J w.r.t. vector $\mathbf{g}$ as

$$\frac{\partial J}{\partial \mathbf{g}} = 2\mathbf{F}^{\mathrm{T}}(\mathbf{Fg}-\mathbf{h}) + 2\lambda\mathbf{g} = 0.$$

Therefore the optimal solution is $\mathbf{g} = \left(\mathbf{F}^{\mathrm{T}}\mathbf{F}+\lambda\mathbf{I}\right)^{-1}\mathbf{F}^{\mathrm{T}}\mathbf{h}$. For the sake of simplicity, let us denote vector $\mathbf{F}^{\mathrm{T}}\mathbf{h}$ by $\mathbf{r}$ and the symmetric matrix $\mathbf{F}^{\mathrm{T}}\mathbf{F}$ by $\mathbf{L}$. Then $\mathbf{g} = (\mathbf{L}+\lambda\mathbf{I})^{-1}\mathbf{r}$. Finally, constraint $\mathbf{g}^{\mathrm{T}}\mathbf{g} = 1$ has to be considered as

$$\mathbf{r}^{\mathrm{T}}(\mathbf{L}+\lambda\mathbf{I})^{-\mathrm{T}}(\mathbf{L}+\lambda\mathbf{I})^{-1}\mathbf{r} = 1. \tag{9}$$

The inverse matrix can be written as

$$(\mathbf{L}+\lambda\mathbf{I})^{-1} = \frac{\mathrm{adj}\,(\mathbf{L}+\lambda\mathbf{I})}{\det(\mathbf{L}+\lambda\mathbf{I})},$$

where $\mathrm{adj}\,(\mathbf{L}+\lambda\mathbf{I})$ and $\det(\mathbf{L}+\lambda\mathbf{I})$ denote the adjoint matrix [3] and the determinant of matrix $\mathbf{L}+\lambda\mathbf{I}$, respectively. This can be substituted into Eq. 9 as follows:

$$\mathbf{r}^{\mathrm{T}}\mathrm{adj}^{\mathrm{T}}(\mathbf{L}+\lambda\mathbf{I})\,\mathrm{adj}\,(\mathbf{L}+\lambda\mathbf{I})\,\mathbf{r} = \det^2(\mathbf{L}+\lambda\mathbf{I}).$$

[3] Adjoint matrix is also called as the matrix of cofactors.

Both sides of the equation contain polynomials. The degrees of the left and right sides are $2n-2$ and $2n$, respectively. If the expression in the sides are subtracted by each other, a polynomial of degree $2n$ is obtained. Note that $n=2$ in the discussed case, when the single angle of a rotation is estimated. The optimal solution is obtained as the real roots of this polynomial. The vector corresponding to the estimated λ_i ,$i \in \{1,2\}$, is calculated as $\mathbf{g}_i = (\mathbf{L}+\lambda_i\mathbf{I})^{-1}\mathbf{r}$. Then the vector with minimal norm $\|\mathbf{F}\mathbf{g}_i - \mathbf{h}\|$ is selected as the optimal solution for the problem.